

Sequence-based Gaussian network model for protein dynamics

Hua Zhang^{1,*} and Lukasz Kurgan²¹School of Computer and Information Engineering, Zhejiang Gongshang University, Hangzhou, Zhejiang 310018, P.R. China and ²Department of Electrical and Computer Engineering, University of Alberta, Edmonton, Alberta T6G 2V4, Canada

Associate Editor: Anna Tramontano

ABSTRACT

Motivation: Gaussian network model (GNM) is widely adopted to analyze and understand protein dynamics, function and conformational changes. The existing GNM-based approaches require atomic coordinates of the corresponding protein and cannot be used when only the sequence is known.**Results:** We report, first of its kind, GNM model that allows modeling using the sequence. Our linear regression-based, parameter-free, sequence-derived GNM (L-pfSeqGNM) uses contact maps predicted from the sequence and models local, in the sequence, contact neighborhoods with the linear regression. Empirical benchmarking shows relatively high correlations between the native and the predicted with L-pfSeqGNM B-factors and between the cross-correlations of residue fluctuations derived from the structure- and the sequence-based GNM models. Our results demonstrate that L-pfSeqGNM is an attractive platform to explore protein dynamics. In contrast to the highly used GNMs that require protein structures that number in thousands, our model can be used to study motions for the millions of the readily available sequences, which finds applications in modeling conformational changes, protein–protein interactions and protein functions.**Contact:** zerozhua@126.com**Supplementary information:** Supplementary data are available at *Bioinformatics* online.

Received on July 29, 2013; revised on November 16, 2013; accepted on December 7, 2013

1 INTRODUCTION

Protein dynamics, which is associated with ever-present thermal fluctuations of atoms and other types of motions that span between rapid (picoseconds) vibrations and relatively slow (microseconds to seconds) movements (Atilgan *et al.*, 2001), implements various important biological processes and functions (Bakan and Bahar, 2009; Bahar and Rader, 2005). The X-ray crystallography studies provide information about the thermal motion, which is represented by the Debye–Waller temperature factors or B-factors. B-factors are proportional to the mean square fluctuations of atomic positions in a crystal due to the thermal motion and positional disorder. They have been studied from a variety of viewpoints in the context of protein function (Bhalla *et al.*, 2006; Jiang *et al.*, 2011) and their relation with conformational changes on protein–protein interactions (Dobbins *et al.*, 2008; Eisenmesser *et al.*, 2005), to name just a

few. Consequently, the knowledge of B-factors provides important insights into the functional dynamics of proteins.

Several computational and physical models have been proposed to predict the B-factors from protein structures (Erman, 2006; Halle, 2002), electron density maps (Ming *et al.*, 2002) and sequences (Schlessinger and Rost, 2005; Yuan *et al.*, 2005; Zhang *et al.*, 2009). To overcome the high computational cost of molecular dynamic simulations (Rueda *et al.*, 2007), several structure-based computational approaches, such as the coarse-grained models including normal mode analysis (Bahar and Rader, 2005), elastic network model (ENM) (Yang *et al.*, 2007a), packing density (Halle, 2002) and weighted contact number (Lin *et al.*, 2008) were developed. The ENMs, including the isotropic Gaussian network model (GNM) (Bahar *et al.*, 1997; Kundu *et al.*, 2002) and the anisotropic network model (Atilgan *et al.*, 2001), define spring-like interactions between residues that are within a certain cutoff distance. They simplify the computationally costly all-atom potentials into a quadratic function in the vicinity of the native state, which allows the decomposition of the motions into vibrational modes with different frequencies, which are known as normal modes. They can determine the (concerted) collective motions of residues that correspond to the lowest-frequency modes comprising large parts of a given protein (Bahar *et al.*, 1999). Being simple and efficient, ENM and GNM have been widely applied to study many motion problems, such as the molecular mechanisms of the GroEL–GroES function (Keskin *et al.*, 2002), motor-protein motions (Zheng and Doniach, 2003) and general conformational changes and functions (Bakan and Bahar, 2009; Haliloglu and Erman, 2009; Haliloglu *et al.*, 2008; Jiang *et al.*, 2011; Kurkcuglu and Bates, 2010; Marcos *et al.*, 2011; Srivastava and Granek, 2013; Szarecka *et al.*, 2007; Tuzmen and Erman, 2011; Wieninger *et al.*, 2011; Yang and Bahar, 2005; Yang *et al.*, 2007b; Yang *et al.*, 2008; Zheng and Brooks, 2005; Zhu and Hummer, 2010; Zhuravleva *et al.*, 2007). Moreover, several variations of the classical ENMs (i.e. the classical GNMs and anisotropic network models) (Atilgan *et al.*, 2001; Kundu *et al.*, 2002) have been developed for better modeling of protein dynamics (Erman, 2006; Kim *et al.*, 2011; Mendez and Bastolla, 2010; Song and Jernigan, 2007; Yang *et al.*, 2009; Zheng, 2008, 2010). However, these methods require the knowledge of protein structure, which limits their applications to thousands of known structures, in contrast to the millions of known non-redundant protein sequences.

The sequence-based predictors use only the protein sequences as their input and thus, they are suitable for the analysis of the

*To whom correspondence should be addressed.

chains with unknown structures. Yuan *et al.* (2005) applied support vector regression to predict the B-factors using position-specific scoring matrix generated from the input sequence. Schlessinger and Rost (2005) proposed a neural network model that uses evolutionary information and solvent accessibility that are generated and predicted from the input chain, respectively. Zhang *et al.* (2009) used the linear regression to investigate the local impact of solvent accessibility on the residue flexibility. Recently, Hirose *et al.* (2010) developed a random forest-based model that uses the input sequence and the predicted secondary structure and solvent accessibility, and Bornot *et al.* (2011) used a sequence fragment matching-based approach to model the protein flexibility. Nevertheless, the main drawback of these sequence-based predictors is that they predict only the B-factor values of the C_α atoms, and they do not provide the information about the collective motions.

Motivated by recent advances in high-throughput sequencing and lagging of the current structure determination pipelines, a sequence-based model would be invaluable to advance our understanding of protein motion and flexibility. We address this need by proposing a novel sequence-based GNM (SeqGNM) that uses contact maps predicted from the sequences with the NNcon method (Tegge *et al.*, 2009). Furthermore, inspired by a finding that strength of the relation between solvent accessibility and flexibility of residues improves when considering a local neighborhood in the sequence (Zhang *et al.*, 2009) and the development of the local contact density model (Halle, 2002), we enhance SeqGNM by using a linear regression that quantifies relation between the local predicted contacts and the flexibility. We illustrate the benefits of the SeqGNM by applying it to predict B-factors and collective motions of residues. We demonstrate that results from SeqGNM are comparable with the outputs from the structure-based GNMs.

2 METHODS

2.1 Datasets and input data

We use a benchmark dataset that was developed in Yang *et al.* (2009) and filtered using Protein Data Bank (PDB)-REPRDB (Noguchi and Akiyama, 2003). It includes 972 protein chains extracted from the PDB (Berman *et al.*, 2000) that have length ≥ 60 , pairwise sequence identity $\leq 25\%$ and high-quality (resolution $\leq 2.0 \text{ \AA}$ and R-factor ≤ 0.2) X-ray structures (to derive reliable values of the native B-factors). Similarly, as in Zhang *et al.* (2009), the average correlation coefficient (ACC) was used to evaluate the performance of various models.

We use NNcon (Tegge *et al.*, 2009) to predict contact maps from protein chains, which are used as inputs to derive the SeqGNM. Prediction of protein contact map is an active research topic, and a number of residue-residue contact predictors have been developed including SVMcon (Cheng and Baldi, 2007), NNcon (Tegge *et al.*, 2009), ProC_S3 (Li *et al.*, 2011), DNCON (Eickholt and Cheng, 2012), CMAPpro (Di Lena *et al.*, 2012), CNNcon (Ding *et al.*, 2013), PhyCMAP (Wang and Xu, 2013) and so forth. We selected NNcon because only this method has a standalone version that can be used for large-scale predictions and provides contact predictions for all residue pairs in the input sequence; other predictors have no standalone versions or output only a part of the inter-residue contact predictions, such as the top L or L/2 predictions. The NNcon method limits the maximum size of the input chain to 800 residues, and consequently, 21 chains from the

benchmark dataset that were longer than 800 were removed. The final dataset includes 951 proteins and is named as PDB951.

We also prepared another independent (dissimilar to the proteins that were used to build NNcon and in the PDB951 dataset that is used to design models) dataset. This dataset includes sequences that were solved by X-ray crystallography and that were deposited in PDB between January 2012 and September 2013, i.e. after PDB951 dataset was collected and after the NNcon method was released. Next, NCBI's BLASTCLUST (Altschul *et al.*, 1997) with the local identity threshold at 25% ($-S 25$) was applied to the union of this set, the PDB951 dataset and the training dataset used to develop NNcon. The independent dataset was constructed by selecting one chain with length between 60 and 800 residues, resolution $\leq 2.0 \text{ \AA}$ and R-factor ≤ 0.2 from each cluster that contains no sequences from the PDB951 dataset and the training set used in the NNcon method. Consequently, this dataset, called PDB748, includes 748 chains that have local identity of at most 25% with each other and also with the protein chains from the PDB951 dataset and the NNcon's training dataset. When testing on the PDB748 dataset, our model is built using proteins from the PDB951 dataset. The PDB IDs of chains included in the PDB951 and PDB748 datasets are provided in the Supplementary Tables S2 and S3, respectively.

2.2 Calculation of normalized B-factors

Experimental B-factor of an atom is defined as $8\pi^2\langle u^2 \rangle$ using the isotropic mean square displacement, u^2 , averaged over the lattice. As the B-factor values depend on the experimental resolution, crystal contacts and the refinement procedures, they are normalized between structures. Following (Schlessinger and Rost, 2005; Zhang *et al.*, 2009), the B-factors of the C_β atoms (C_α atoms for Gly) for each chain were normalized as $B' = (B - AVE)/\sigma$, where B is the native B-factor, AVE is the average native B-factor in a given chain and σ is the standard deviation of native B-factors for all C_β atoms (C_α atoms for Gly) in a given chain.

2.3 Gaussian network model and parameter-free GNM

Each protein in GNM is modeled by an elastic network, where the springs connecting the nodes represent the bonded and non-bonded interactions between the pairs of residues located within a cutoff distance R_C (Kundu *et al.*, 2002). Assuming that the fluctuations between residues are isotropic and Gaussian, the potential of the network of N nodes (residues) is

$$V_{GNM} = \frac{\gamma}{2} \sum_{i,j} \Gamma_{ij} (\mathbf{R}_{ij} - \mathbf{R}_{ij}^0)^2 \quad (1)$$

where \mathbf{R}_{ij} and \mathbf{R}_{ij}^0 are instantaneous and original distance vectors between residues i and j , respectively, γ is the force constant that is assumed to be uniform for all network springs and $\Gamma = (\Gamma_{ij})$ is the following Kirchhoff matrix based on the contact information:

$$\Gamma_{ij} = \begin{cases} -1, & \text{if } i \neq j \text{ and } R_{ij}^0 \leq R_C \\ 0, & \text{if } i \neq j \text{ and } R_{ij}^0 > R_C \\ -\sum_{j \neq i} \Gamma_{ij}, & \text{if } i = j \end{cases} \quad (2)$$

where R_{ij}^0 is the distance between residues i and j . Then, the mean square fluctuation of the i th residue is given by

$$\langle \Delta \mathbf{R}_i^2 \rangle = (3k_B T / \gamma) [\Gamma^{-1}]_{ii} \quad (3)$$

where k_B is the Boltzmann constant, T is temperature and γ is a constant scaling factor. The cross-correlation map, which includes the mean correlations between residue fluctuations, is given by

$$\langle \Delta \mathbf{R}_i \cdot \Delta \mathbf{R}_j \rangle = (3k_B T / \gamma) [\Gamma^{-1}]_{ij} \quad (4)$$

Furthermore, Yang *et al.* (2009) proposed parameter-free GNM (pfGNM) that replaces the cutoff distance R_C by introducing a more physical concept of inverse power dependence for the residue–residue interactions. In pfGNM, the elements of the Kirchhoff matrix are calculated as

$$\Gamma_{ij}^{pf} = \begin{cases} R_{ij}^{-2} & \text{if } i \neq j \\ -\sum_{j \neq i} \Gamma_{ij}^{pf} & \text{if } i = j \end{cases} \quad (5)$$

where R_{ij} is the distance between residues i and j .

2.4 Sequence-based Gaussian network models

In this work, the GNM is calculated from the sequence-predicted contact maps that are generated with the NNcon method (Tegge *et al.*, 2009). NNcon provides probability values $P_{ij} \in [0, 1]$ that express the strength of the contact between C_β atoms (C_α atoms for Gly) of residues i and j . Similar to the classical GNM and the pfGNM, the corresponding two types of the SeqGNMs are proposed. One is based on the probability cutoff P_C and the other directly uses the probability values to construct the Kirchhoff matrix. The Kirchhoff matrix of the classical SeqGNM is defined as

$$\Gamma_{ij}^{Seq} = \begin{cases} -1, & \text{if } i \neq j \text{ and } P_{ij} \leq P_C \\ 0, & \text{if } i \neq j \text{ and } P_{ij} > P_C \\ -\sum_{j \neq i} \Gamma_{ij}^{Seq}, & \text{if } i = j \end{cases} \quad (6)$$

and the Kirchhoff matrix of the parameter-free sequence-based pfGNM (pfSeqGNM) is defined as

$$\Gamma_{ij}^{pfSeq} = \begin{cases} -P_{ij}, & \text{if } i \neq j \\ -\sum_{j \neq i} \Gamma_{ij}^{pfSeq}, & \text{if } i = j \end{cases} \quad (7)$$

2.5 Linear regression models

As shown in Erman (2006), the Kirchhoff matrix Γ in GNM could be written as $\Gamma = D + U$, where D and U are the matrices of the diagonal and off-diagonal elements, respectively. Furthermore, the inverse $\Gamma^{-1} = (D + U)^{-1}$ could be written in the form of Taylor series expansion: $\Gamma^{-1} = D^{-1} - D^{-1}U D^{-1} + \dots$. As a result, the diagonal component D^{-1} quantifies the main contribution of the local packing density to Γ^{-1} . The second term, $D^{-1}U D^{-1}$, provides a relatively weak contribution resulting from the positional correlations among different residue pairs. Moreover, Halle (2002) proposed the local density model, where only the contributions of diagonal terms are considered. Based on their findings (Erman, 2006; Halle, 2002), we use a linear regression model to investigate the local impact of the diagonal terms of Γ^{pfSeq} on the performance of B-factor prediction. The flexibility of the i th residue, which is located at the center of a window that defines local neighborhood, denoted as B'-factor, is defined as

$$\hat{B}'_i = \sum_{k=-h}^h w_k \Gamma_{i+k,i+k}^{pfSeq} + b \quad (8)$$

where b is the intercept, weights w_k are determined using the least squares fit between the estimated and the native B'-factor values and the window includes $2h+1$ residues, where $h=0,1,2,\dots$. This linear model is empirically shown to improve the B'-factor prediction when compared with the case in which only the diagonal terms are used. Furthermore, the w_k weights learned from the PDB951 dataset with optimal window size h are used to construct a new Kirchhoff matrix, which is empirically shown to improve the B'-factor predictions when compared with the GNM that does not use this extension (see Section 3). This extended model also allows the calculation of the cross-correlations of the residue

fluctuations. The Linear regression-based, parameter-free, Sequence-derived GNM (L-pfSeqGNM) is defined as

$$\Gamma_{ij}^{L-pfSeq} = \begin{cases} \sum_{k=-h}^h w_k \Gamma_{i+k,j+k}^{pfSeq}, & \text{if } i \neq j \\ -\sum_{j \neq i} \Gamma_{ij}^{L-pfSeq}, & \text{if } i = j \end{cases} \quad (9)$$

where $\Gamma_{i+k,j+k}^{pfSeq} = 0$ when $i+k \leq 0$, $j+k \leq 0$ or $i+k \geq N+1$, $j+k \geq N+1$ and N is the length of the protein chain.

3 RESULTS

3.1 Impact of the contact prediction probability cutoffs on the prediction of residue flexibility with SeqGNM

The NNcon method, which generates inputs for SeqGNM, provides predicted probability values for the residue–residue contacts. Motivated by the assessments of the residue–residue contact predictions in Critical Assessment of Protein Structure Prediction (CASP) (Monastyrskyy *et al.*, 2011), NNcon (Tegge *et al.*, 2009) defines contacts between C_β (C_α for Gly) atoms using two thresholds at 8 and 12 Å; other thresholds are not considered. We use the classical GNM that applies binary contacts, where the contact probabilities are binarized using varying cutoffs that are shown on the x -axis in Figure 1. The ACC values between the predicted and the native B'-factors (shown on the y -axis in Fig. 1) are higher when defining the contacts at 12 Å, and thus, we select this definition throughout all subsequent results. Binarization of the probabilities predicted by NNcon with cutoff at 0.3, i.e. a given pair of residues is in contact when the probability > 0.3 , leads to ACC value equals 0.456, which indicates relatively good correlation.

3.2 Evaluation of the pfSeqGNM

Moreover, based on the work in Yang *et al.* (2009), we developed the pfSeqGNM, where the original probability values, instead of the binary values, are used as the inputs. The pfSeqGNM method obtains ACC equals 0.493 based on the PDB951 dataset, which improves by 0.04 over the classical SeqGNM. This concurs with Yang *et al.* (2009), where the structure-based parameter-free model, pfGNM, was shown to outperform the classical structure-based GNM.

3.3 Use of local predicted contacts improves prediction of residue flexibility with pfSeqGNM

Inspired by Erman (2006) and Halle (2002), we investigate whether the local predicted contacts, i.e. contacts in a sequence

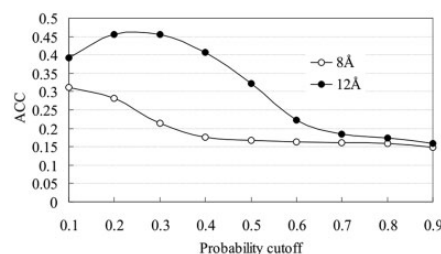


Fig. 1. The ACCs between the native B'-factors and the B'-factors predicted with the classical SeqGNM on the PDB951 dataset. The ACC values are calculated for varying probability cutoffs

window, contribute to the flexibility expressed using B'-factors. We developed linear regression model that takes the predicted probability values of contacts, i.e. the diagonal elements in the Kirchhoff matrix in the window as its input to compute the B'-factor value of the central residue. Figure 2 shows the ACC values that quantify the correlations between the outputs of the linear regression model and the native B'-factor values for the window sizes (shown on the x-axis) between 1 and 21 residues. These results are based on 5-fold cross-validation (CV) (Zhang *et al.*, 2009) (Fig. 2A) and 10-fold cross-validation (Fig. 2B) on the PDB951 dataset. The results for the 5-fold CV and 10-fold CV are similar. For the 5-/10-fold CV, the ACC values improve from 0.479/0.478, which corresponds to the window size of one when the local neighborhood is not used, to 0.516/0.515 that corresponds to the window size of seven. Use of larger window sizes does not lead to further improvements. Consequently, the window size of seven is selected. The corresponding linear regression model, which is trained on the entire PDB951 dataset, is as follows:

$$\hat{B}_i = 0.0579 \times \Gamma_{i-3,i-3}^{\text{pfSeq}} + 0.0357 \times \Gamma_{i-2,i-2}^{\text{pfSeq}} + 0.0512 \times \Gamma_{i-1,i-1}^{\text{pfSeq}} + 0.2722 \times \Gamma_{i,i}^{\text{pfSeq}} + 0.0722 \times \Gamma_{i+1,i+1}^{\text{pfSeq}} + 0.0230 \times \Gamma_{i+2,i+2}^{\text{pfSeq}} + 0.0569 \times \Gamma_{i+3,i+3}^{\text{pfSeq}} + 0.0186 \quad (10)$$

where $\Gamma_{i,i}^{\text{pfSeq}}$ is defined in Equation (7), and the window includes three residues on both sides of the i th position. The regression model has the largest coefficient for the central, i th residue, which implies that, as expected, the contacts of this residue have the strongest relation with its flexibility. The coefficients for the neighboring residues are also positive, and they indicate that the contacts of these residues have influence on the flexibility of the i th residue.

We use this linear regression model to create a new Kirchhoff matrix that is expressed in Equation (9), and the corresponding GNM is referred to as the L-pfSeqGNM.

3.4 Comparative evaluation of the sequence- and structure-based prediction of residue flexibility

Table 1 shows the ACC values between the native B'-factors and B'-factors predicted with two structure-based methods, the classical GNM and the pfGNM, and with two sequence-based methods, pfSeqGNM and L-pfSeqGNM. The predictions were

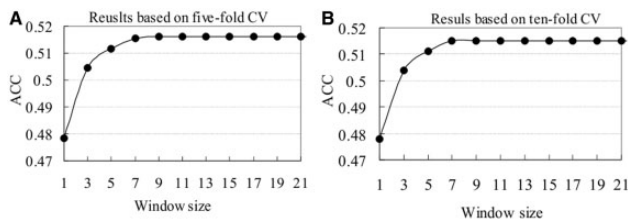


Fig. 2. Strength of the relation between native B'-factors and the B'-factors predicted using the linear regression model computed from the local predicted contacts, which is measured with the ACCs (y-axis). The ACC values are calculated for varying window sizes (x-axis) based on 5-fold cross-validation (panel A) and 10-fold cross-validation (panel B) on the PDB951 dataset

performed on the PDB951 and PDB748 datasets, and the corresponding ACC values are reported in the upper triangle and the lower triangle in Table 1, respectively. The ACC value of pfGNM is better than that of GNM for both datasets, which agrees with Yang *et al.* (2009). Similarly, ACC of L-pfSeqGNM is higher than that of pfSeqGNM, which confirms that the local predicted contacts contribute to the prediction of residue flexibility. The strong correlation of 0.94 between pfGNM and GNM implies that these two structure-based methods generate similar results. Analogous similarity is observed between L-pfSeqGNM and pfSeqGNM, for which the predictions are correlated with ACC at 0.93. This is a consequence of the fact that the former approach extends the latter on by using a linear model. Importantly, the difference in the predictive quality between structure-based and sequence based methods is relatively small. The ACC of L-pfSeqGNM (0.52 and 0.53 on the PDB951 and PDB748 datasets, respectively) is close to that of GNM (0.56 and 0.58), on both datasets showing moderate correlations between the predicted and native B'-factors.

Moreover, the structure-based methods (GNM and pfGNM) and the sequence-based methods (pfSeqGNM and L-pfSeqGNM) have correlations at round 0.6, which suggests that the sequence-based methods generate results that are relatively similar to the structure-based methods. We plotted the distributions of the correlation coefficient values of each sequence between the outputs of pfGNM and pfSeqGNM on the PDB951 and PDB748 datasets; see Figure 3. We note that the distributions for the PDB951 and PDB748 datasets are similar and that the majority of sequences have correlation coefficient values between 0.5 and 0.8, i.e. 83% of sequences in each of the two datasets. Although the predictions generated by the structure-based methods are better than those of the sequence-based methods, the latter methods can be applied to a much wider range of problems where the structural information is unavailable.

3.5 Impact of the predictive quality of NNcon on the prediction of residue flexibility with L-pfSeqGNM

The assessment of contact prediction uses two metrics, the accuracy (Acc) and the coverage (Cov), which are widely used to

Table 1. The ACCs between the native B'-factors (NBF) and the B'-factors predicted by the structure-based GNM and pfGNM methods, and by the sequence-based pfSeqGNM and L-pfSeqGNM methods

Method	NBF	GNM	pfGNM	pfSeqGNM	L-pfSeqGNM
NBF	1	0.557	0.593	0.493	0.517
GNM	0.584	1	0.940	0.592	0.589
pfGNM	0.621	0.941	1	0.635	0.627
pfSeqGNM	0.497	0.576	0.623	1	0.927
L-pfSeqGNM	0.526	0.587	0.625	0.927	1

Note: The predictions were performed on the PDB951 and PDB748 datasets; the corresponding ACC values are reported in the upper and the lower triangle, respectively. The results in the last column, i.e. the ACCs between B'-factors predicted by L-pfSeqGNM and other methods, are based on the 5-fold cross-validation on the PDB951 dataset; the results using 10-fold CV are not shown, as they are virtually identical.

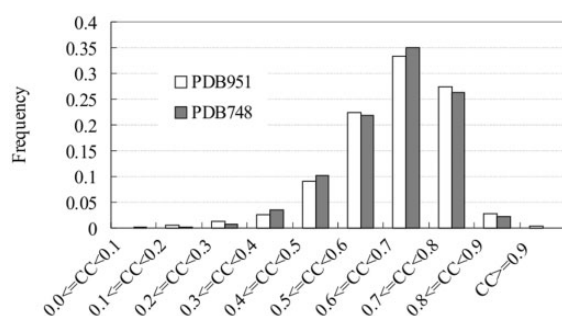


Fig. 3. The distributions of CC values between the outputs of pfGNM and pfSeqGNM for individual sequences on the PDB951 and PDB748 datasets. The frequencies/fractions of sequences are shown using CC values binned using 0.1 wide intervals

evaluate the contact predictions in the CASP and the recent studies (Di Lena *et al.*, 2012; Eickholt and Cheng, 2012; Li *et al.*, 2011; Tegge *et al.*, 2009). The accuracy is defined as the number of correctly predicted residue–residue contacts divided by the total number of top $L/5$ or L contact predictions, where L is the length of the protein in residues. The coverage is the number of correctly predicted residue–residue contacts divided by the number of true contacts. The contact evaluation is commonly divided into three categories: short-range contacts for which residue separation in sequence is ≥ 6 and <12 , medium-range contacts with separation ≥ 12 and <24 and long-range contacts that are defined as having separation ≥ 24 residues. Table 2 shows the predictive performance of the NNcon method for short, medium and long-range contact prediction on the PDB951 dataset. The accuracy (Acc) values for the distance cutoff of 8 Å are close to the results reported in recent studies (Di Lena *et al.*, 2012; Eickholt and Cheng, 2012; Li *et al.*, 2011; Tegge *et al.*, 2009), but are markedly lower than those of 12 Å case. For the distance cutoff of 12 Å, especially when considering top L predictions, NNcon yields accuracy of 0.750 and coverage of 0.467 for short-range contact, accuracy of 0.481 and coverage of 0.311 for medium-range contact. This result supports our finding that the predicted contacts defined at 12 Å result in better B-factor prediction than the cutoff of 8 Å.

Similarly as in the recent works (Eickholt and Cheng, 2012; Eickholt *et al.*, 2011), we also calculated the number of contact predictions that are close to a true contact. A predicted contact is considered correct if a true residue–residue contact is within $\pm\sigma$ residues for small values of σ . For example, for $\sigma = 1$, a predicted contact (i, j) is assumed correct if a true contact is at positions (i, j) , $(i \pm 1, j)$, $(i, j \pm 1)$ and $(i \pm 1, j \pm 1)$. Table 2 lists the predictive performance of NNcon on the PDB951 dataset for $\sigma = 1$ and $\sigma = 2$. The results demonstrate that if an offset by one or two residue is allowed ($\sigma = 1$ or 2), both the accuracy and the coverage are improved by a substantial margin. In the case of assessing the top L contact predictions and when $\sigma = 2$, the NNcon predictor yields relatively high accuracies of 0.991, 0.857 and 0.639 for the short-, medium- and long-range contacts, respectively. We note that GNM and its variations use the local, in the sequence, residue–residue contacts. The fact that the contact predictions are rather accurate when allowing small offsets, which are within the range of the residues used by these methods,

Table 2. The predictive performance of NNcon for short, medium and long-range contact predictions on the PDB951 dataset with the distance cutoffs of 8 Å and 12 Å, respectively

Evaluation criteria	Contact range	8 Å		12 Å	
		Acc	Cov	Acc	Cov
Top $L/5$	Short	0.408	0.253	0.892	0.111
	Medium	0.321	0.153	0.642	0.084
	Long	0.199	0.029	0.463	0.017
Top $L/5$, $\sigma = 1$	Short	0.776	0.511	0.980	0.124
	Medium	0.560	0.304	0.864	0.116
	Long	0.362	0.054	0.650	0.024
Top $L/5$, $\sigma = 2$	Short	0.923	0.606	0.999	0.127
	Medium	0.715	0.371	0.922	0.126
	Long	0.447	0.068	0.712	0.027
Top L	Short	0.203	0.620	0.750	0.467
	Medium	0.170	0.398	0.481	0.311
	Long	0.119	0.088	0.352	0.062
Top L , $\sigma = 1$	Short	0.581	0.998	0.949	0.603
	Medium	0.407	0.883	0.765	0.507
	Long	0.260	0.196	0.558	0.099
Top L , $\sigma = 2$	Short	0.826	1.000	0.991	0.631
	Medium	0.555	0.973	0.857	0.570
	Long	0.351	0.265	0.639	0.114

Note: Value of σ determines an offset by σ positions in the sequence that is allowed to consider a given prediction correct.

explains the relatively high correlations between the native B-factors and the B-factors predicted by the sequence-based L-pfSeqGNM, and between the outputs of structure-based pfGNM and sequence-based pfSeqGNM. Similar observations are true when evaluating the NNcon predictor on the PDB748 dataset; see Supplementary Table S1.

Figure 4 shows scatter plots of the average accuracy of the NNcon predictor (i.e. the average over the three accuracy values for the short, medium and long contacts for each chain) and the ACC values between the native B'-factors and the B'-factors predicted by L-pfSeqGNM on the PDB951 dataset. The figure demonstrates lack of a strong linear relation between these two metrics when considering evaluations for both the top $L/5$ predictions (Fig. 4A) and for the top L predictions (Fig. 4B). The corresponding Pearson correlation coefficients between the average accuracies of NNcon and the ACC values of L-pfSeqGNM for the top $L/5$ predictions and top L predictions are 0.15 and 0.19, respectively. Moreover, although the NNcon accuracies have a wide range of values, from low at about ~ 0.1 to high values close to 0.9, the corresponding ACC values of L-pfSeqGNM are always fairly high, i.e. significant majority of the values are above >0.4 . These observations demonstrate that the proposed here sequence-based L-pfSeqGNM method does not rely on the high quality of contact maps predicted by NNcon. Our method can predict B-factors with good predictive quality even when the predictions from NNcon have relatively low accuracy; this could be explained by the results in Table 2 that suggest that correct contacts can be found with a small offset in the sequence. A similar relation of the ACC values of

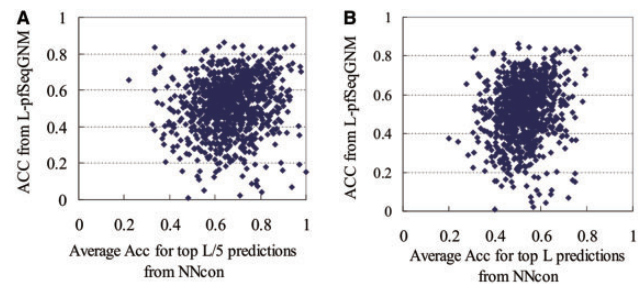


Fig. 4. The scatter plots of the average ACC values (x-axis) from NNcon and ACC values (y-axis) from L-pfSeqGNM with the contact cutoff of 12 Å for top $L/5$ contact predictions (panel A) and top L predictions (panel B). Each point corresponds to one protein from the PDB951 dataset

L-pfSeqGNM with the average Acc values of NNcon is true on the PDB748 dataset, see Supplementary Figure S1.

3.6 Sequence-based determination of collective residue motions

One of the key advantages of the SeqGNM is its ability to generate the cross-correlations of residue fluctuations and to describe the correlated motions of residues in a given protein, particularly when the structure of this protein is unknown. The cross-correlations express the strength of the collective motions for a given pair of residues. They are useful in understanding long-range propagation of motion and large domain movements, which are relevant to protein function. Their applications have been recently widely explored (Bahar *et al.*, 1999; Doruker *et al.*, 2006; Jiang *et al.*, 2011; Marcos *et al.*, 2011). The cross-correlation between any two residues is computed from the Kirchhoff matrix. We compute the ACCs of the cross-correlations of residue fluctuations for all pairs of methods among the considered four GNMs on the PDB951 and PDB748 datasets; see Table 3. The ACC values are >0.7 for both datasets, which indicates that the cross-correlation matrices generated by the four methods are similar. At the same time, the SeqGNMs, i.e. pfSeqGNM and L-pfSeqGNM, can be used to explore the collective motions for proteins with unknown structures, which allows for a wider range of applications and targets.

3.7 Case studies

We demonstrate and compare predictions of the considered sequence- and structure-based GNMs for three proteins: bovine β -lactoglobulin (β lg, PDBid: 1B8E, chain A) (Oliveira *et al.*, 2001), histamine-binding protein from female brown ear *Rhipicephalus appendiculatus* tick (Ra-HBP, PDBid: 1QFT, chain A) (Paesen *et al.*, 1999) and the quorum-sensing protein TraM (PDBid: 1UPG, chain A) (Vannini *et al.*, 2004). β lg is a prominent member of the lipocalin family, a large group of proteins involved in the transport of small hydrophobic molecules, and has been widely used for protein-folding dynamics and aggregation modeling (Arnaudov and de Vries, 2006; Bello *et al.*, 2011, 2012; Krebs *et al.*, 2009) due to its abundant availability in bovine milk. Ra-HBP binds histamine with high affinity and specificity, and the histamine binding proteins are currently

Table 3. The ACCs between the cross-correlations of residue fluctuations generated by the four considered GNMs on the PDB951 and PDB748 datasets; the corresponding ACC values are reported in the upper triangle and the lower triangle, respectively

Method	GNM	pfGNM	pfSeqGNM	L-pfseqGNM
GNM	1	0.810	0.717	0.716
pfGNM	0.813	1	0.955	0.960
pfSeqGNM	0.715	0.954	1	0.993
L-pfSeqGNM	0.716	0.960	0.993	1

Note: The results in the last column, i.e. the ACCs between the cross-correlations of residue fluctuations generated by L-pfSeqGNM and other methods are based on the 5-fold cross-validation; the results based on the 10-fold CV are not shown, as they are virtually identical

investigated as potential therapeutic agents for the treatment of various diseases (Mans, 2005). TraM protein inhibits the activity of its associated LuxR-type transcription factor TraR in several different microbial taxa, and is often required to maintain the quorum-sensing mechanism in the inactive state (Chen *et al.*, 2006, 2007). Ra-HBP shares the same family (i.e. retinol binding protein-like) in the Structural Classification of Proteins (SCOP) database (Murzin *et al.*, 1995) and has low-sequence identity [$<25\%$, measured with BLASTCLUST (Altschul *et al.*, 1997)] with the β lg protein. Moreover, β lg and Ra-HBP have similar B'-factor profiles, whereas the B'-factor profile of the third protein TraM is different from these two proteins, where β lg and the Ra-BHP have several flexible segments and TraM is mostly rigid.

Figure 5 compares the native B'-factor (normalized native B-factor) profiles and the B'-factors predicted with GNM, pfGNM, pfSeqGNM and L-pfSeqGNM. For β lg, the correlation coefficient values between the native B'-factors and the B'-factors predicted with GNM, pfGNM, pfSeqGNM and L-pfSeqGNM are 0.624, 0.648, 0.610 and 0.611, respectively. The coefficients are 0.861, 0.858, 0.558 and 0.658, respectively, for the Ra-BHP. These two results taken together suggest that the proposed SeqGNMs can produce different and high-quality B'-factor profiles for proteins in the same family but with different sequences. Similarly high values of coefficients that equal 0.651, 0.654, 0.788 and 0.769, respectively, were obtained for the TraM protein. These case studies demonstrate that all four B'-factor prediction models correctly identified the flexible regions (regions with the high-positive B'-factor values) and the rigid regions (with low-negative B'-factor values) along the three sequences.

Figures 6, 7 and 8 show correlation maps of residue fluctuations that are computed with the GNM (panel A), pfGNM (panel B), pfSeqGNM (panel C) and L-pfSeqGNM (panel D) methods for the three proteins. The colors range between red (which denoted strong positive correlations) and blue (strong negative correlations). Currently, there are no experimentally derived correlation maps, except for the diagonal terms that correspond to the B-factors, which could be used as a reference. However, the similarity between the four maps (for each of the three proteins) indicates that the SeqGNMs provide a viable alternative to the maps generated from the structure.

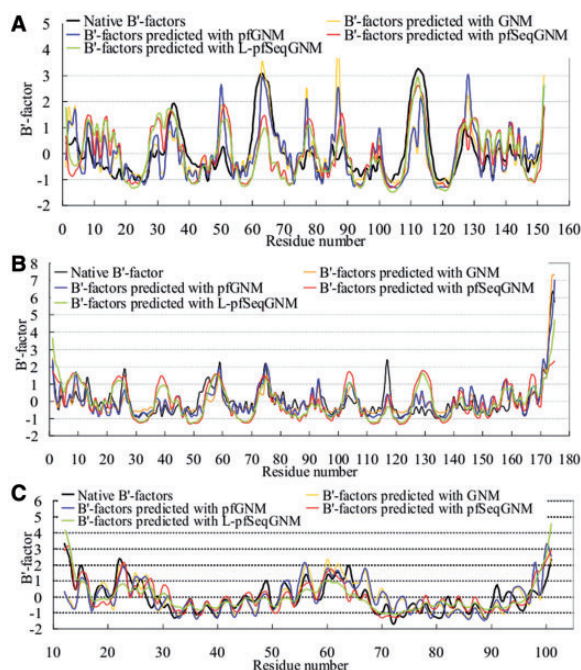


Fig. 5. The native B-factors and the B-factors predicted with the GNM, pfGNM, pfSeqGNM and L-pfSeqGNM methods for (A) β -lactoglobulin (PDBid: 1B8E, chain A), (B) the histamine-binding protein Ra-HBP (PDBid: 1QFT, chain A) and (C) the quorum-sensing protein TraM (PDBid: 1UPG, chain A)

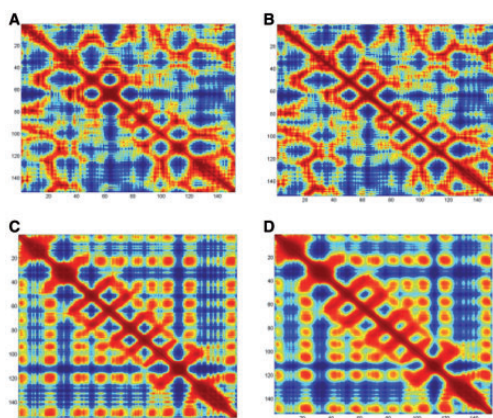


Fig. 6. The maps of the cross-correlations of residue fluctuations for the β -lactoglobulin protein (PDBid: 1B8E, chain A) computed with (A) GNM, (B) pfGNM, (C) pfSeqGNM and (D) L-pfSeqGNM methods. The colors range between red (strong positive correlations) and blue (strong negative correlations)

Although these three case studies should not be taken as typical, they demonstrate (in agreement with our benchmarking results) that SeqGNMs could be applied to provide useful prediction of the B-factors and correlation maps, and that these predictions have comparable quality with the predictions obtained from the structure-based GNMs.

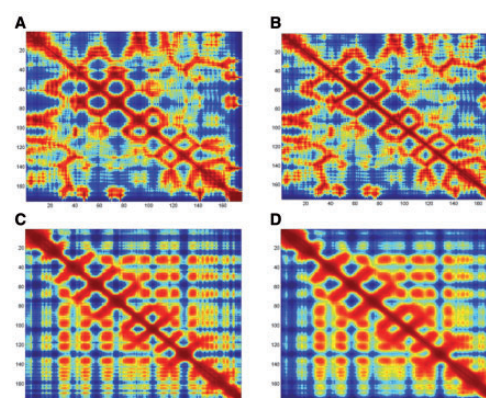


Fig. 7. The maps of the cross-correlations of residue fluctuations for the histamine-binding protein Ra-HBP (PDBid: 1QFT, chain A) computed with (A) GNM, (B) pfGNM, (C) pfSeqGNM and (D) L-pfSeqGNM methods. The colors range between red (strong positive correlations) and blue (strong negative correlations)

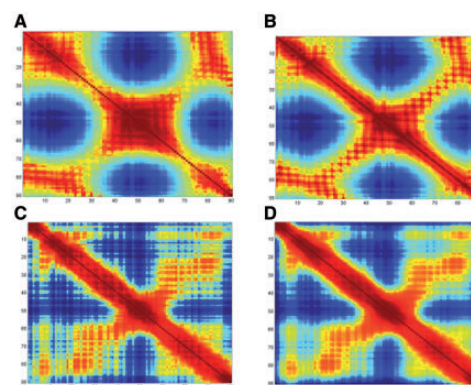


Fig. 8. The maps of the cross-correlations of residue fluctuations for the quorum-sensing protein TraM (PDBid: 1UPG, chain A) computed with (A) GNM, (B) pfGNM, (C) pfSeqGNM and (D) L-pfSeqGNM methods. The colors range between red (strong positive correlations) and blue (strong negative correlations)

4 DISCUSSION

The B-factors reflect the residue fluctuations and static, dynamic and lattice disorders. However, they depend on the experimental resolution, crystal contacts and refinement procedures, which is why the B-factor profiles of homologous protein are shown to be correlated with each other with the ACC of 0.80 (Yuan *et al.*, 2005). This constitutes an approximate upper limit for the prediction of the B-factor values, which applies to the considered GNM-based models. Yang *et al.* (2009) have recently proposed a new distance-dependent (parameter-free) GNM in which residue pairs are weighted by the inverse square of their distances. This pfGNM method had been shown to outperform the classical distance cutoff-based GNM in prediction the B-factors. Here, the proposed SeqGNM methods, pfSeqGNM and L-pfSeqGNM, predict the B-factors with comparably (to the structure-based method) high correlations equal 0.49 and 0.52 on the PDB951 dataset, and 0.50 and 0.53 on the PDB748

dataset, respectively. We demonstrate that the pfGNM is also advantageous for our sequence-based approach, i.e. we show that the pfSeqGNM outperforms the classical SeqGNMs. Furthermore, motivated by the findings concerning the impact of local contact density and local solvent accessibility on the residue flexibility expressed with the B-factors (Halle, 2002; Zhang *et al.*, 2009), we use linear regression to model the relation between the local predicted contacts and the residue flexibility. This led to the development of an improved pfSeqGNM that uses the local contacts, which is called L-pfSeqGNM. Our empirical results suggest that this model provides useful predictions of the residue flexibility and the collective residue motions.

The key advantage of the SeqGNM is that it can be applied to proteins with unknown structures and known sequences, which number in millions. In contrast, the existing and widely adopted structure-based GNMs are limited to a much smaller subpopulation of proteins with known structure. Our model finds numerous applications in modeling of protein motion, conformational changes, protein-protein interactions and protein functions, to name just a few.

ACKNOWLEDGEMENT

The authors would like to thank Dr Cheng for providing the training dataset used in NNcon program.

Funding: National Natural Science Foundation of China (grant no. 61170099 and 610033074 to H.Z.), the Zhejiang Provincial Natural Science Foundation of China (grant no. Y1110840, Y1090165, Y1110644 and Y1110969 to H.Z.) and NSERC Discovery grant (to L.K.).

Conflict of Interest: none declared.

REFERENCES

- Altschul,S.F. *et al.* (1997) Gapped BLAST and PSI-BLAST: a new generation of protein database search programs. *Nucleic Acids Res.*, **25**, 3389–3402.
- Arnaudov,L.N. and de Vries,R. (2006) Strong impact of ionic strength on the kinetics of fibrillar aggregation of bovine β -lactoglobulin. *Biomacromolecules*, **7**, 3490–3498.
- Atilgan,A.R. *et al.* (2001) Anisotropy of fluctuation dynamics of proteins with an elastic network model. *Biophys. J.*, **80**, 505–515.
- Bahar,I. and Rader,A.J. (2005) Coarse-grained normal mode analysis in structural biology. *Curr. Opin. Struct. Biol.*, **15**, 586–592.
- Bahar,I. *et al.* (1997) Direct evaluation of thermal fluctuations in proteins using a single-parameter harmonic potential. *Fold. Des.*, **2**, 173–181.
- Bahar,I. *et al.* (1999) Collective motions in HIV-1 reverse transcriptase: examination of flexibility and enzyme function. *J. Mol. Biol.*, **285**, 1023–1037.
- Bakan,A. and Bahar,I. (2009) The intrinsic dynamics of enzymes plays a dominant role in determining the structural changes induced upon inhibitor binding. *Proc. Natl Acad. Sci. USA*, **106**, 14349–14354.
- Bello,M. *et al.* (2011) Energetics of ligand recognition and self-association of bovine β -lactoglobulin: differences between variants A and B. *Biochemistry*, **50**, 151–161.
- Bello,M. *et al.* (2012) Structure and dynamics of β -lactoglobulin in complex with dodecyl sulfate and laurate: a molecular dynamics study. *Biophys. Chem.*, **165**–**166**, 79–86.
- Berman,H.M. *et al.* (2000) The protein data bank. *Nucleic Acids Res.*, **28**, 235–242.
- Bhalla,J. *et al.* (2006) Local flexibility in molecular function paradigm. *Mol. Cell. Proteomics*, **5**, 1212–1223.
- Bornot,A. *et al.* (2011) Predicting protein flexibility through the prediction of local structures. *Proteins*, **79**, 839–852.
- Chen,G. *et al.* (2006) Crystal structure and mechanism of TraM2, a second quorum-sensing antiactivator of *Agrobacterium tumefaciens* strain A6. *J. Bacteriol.*, **188**, 8244–8251.
- Chen,G. *et al.* (2007) Structural basis for antiactivation in bacterial quorum sensing. *Proc. Natl Acad. Sci. USA*, **104**, 16474–16479.
- Cheng,J. and Baldi,P. (2007) Improved residue contact prediction using support vector machines and a large feature set. *BMC Bioinformatics*, **8**, 113.
- Ding,W. *et al.* (2013) CNNcon: improved protein contact maps prediction using cascaded neural networks. *PLoS One*, **8**, e61533.
- Dobbins,S.E. *et al.* (2008) Insights into protein flexibility: the relationship between normal modes and conformational change upon protein-protein docking. *Proc. Natl Acad. Sci. USA*, **105**, 10390–10395.
- Doruker,P. *et al.* (2006) Collective dynamics of EcoRI-DNA complex by elastic network model and molecular dynamics simulations. *J. Biomol. Struct. Dyn.*, **24**, 1–16.
- Eickholt,J. and Cheng,J. (2012) Predicting protein residue-residue contacts using deep networks and boosting. *Bioinformatics*, **28**, 3066–3072.
- Eickholt,J. *et al.* (2011) A conformation ensemble approach to protein residue-residue contact. *BMC Struct. Biol.*, **11**, 38.
- Eisenmesser,E.Z. *et al.* (2005) Intrinsic dynamics of an enzyme underlies catalysis. *Nature*, **438**, 117–121.
- Erman,B. (2006) The gaussian network model: precise prediction of residue fluctuations and application to binding problems. *Biophys. J.*, **91**, 3589–3599.
- Haliloglu,T. *et al.* (2008) Prediction of binding sites in receptor-ligand complexes with the Gaussian network model. *Phys. Rev. Lett.*, **100**, 228102.
- Haliloglu,T. and Erman,B. (2009) Analysis of correlations between energy and residue fluctuations in native proteins and determination of specific sites for binding. *Phys. Rev. Lett.*, **102**, 088103.
- Halle,B. (2002) Flexibility and packing in proteins. *Proc. Natl Acad. Sci. USA*, **99**, 1274–1279.
- Hirose,S. *et al.* (2010) Prediction of protein motions from amino acid sequence and its application to protein-protein interaction. *BMC Struct. Biol.*, **10**, 20.
- Jiang,J. *et al.* (2011) Large collective motions regulate the functional properties of glutamate transporter trimers. *Proc. Natl Acad. Sci. USA*, **108**, 15141–15146.
- Keskin,O. *et al.* (2002) Molecular mechanisms of chaperonin GroEL-GroES function. *Biochemistry*, **41**, 491–501.
- Kim,J.I. *et al.* (2011) Domain decomposition-based structural condensation of large protein structures for understanding their conformational dynamics. *J. Comput. Chem.*, **32**, 161–169.
- Krebs,M.R. *et al.* (2009) Amyloid fibril-like structure underlies the aggregate structure across the pH range for β -lactoglobulin. *Biophys. J.*, **96**, 5013–5019.
- Kundu,S. *et al.* (2002) Dynamics of proteins in crystals: comparison of experiment with simple models. *Biophys. J.*, **83**, 723–732.
- Kurkcuoglu,O. and Bates,P.A. (2010) Mechanism of cohesin loading onto chromosomes: a conformational dynamics study. *Biophys. J.*, **99**, 1212–1220.
- Di Lena,P. *et al.* (2012) Deep architectures for protein contact map prediction. *Bioinformatics*, **28**, 2449–2457.
- Li,Y. *et al.* (2011) Predicting residue-residue contacts using random forest models. *Bioinformatics*, **27**, 3379–3384.
- Lin,C.P. *et al.* (2008) Deriving protein dynamical properties from weighted protein contact number. *Proteins*, **72**, 929–935.
- Mans,B.J. (2005) Tick histamine-binding proteins and related lipocalins: potential as therapeutic agents. *Curr. Opin. Investig. Drugs*, **6**, 1131–1135.
- Marcos,E. *et al.* (2011) Changes in dynamics upon oligomerization regulate substrate binding and allostery in amino acid kinase family members. *PLoS Comput. Biol.*, **7**, e1002201.
- Mendez,R. and Bastolla,U. (2010) Torsional network model: normal modes in torsion angle space better correlate with conformation changes in proteins. *Phys. Rev. Lett.*, **104**, 228103.
- Ming,D. *et al.* (2002) How to describe protein motion without amino acid sequence and atomic coordinates. *Proc. Natl Acad. Sci. USA*, **99**, 8620–8625.
- Monastyrskyy,B. *et al.* (2011) Evaluation of residue-residue contact predictions in CASP9. *Proteins*, **79** (Suppl. 10), 119–125.
- Murzin,A.G. *et al.* (1995) SCOP: a structural classification of proteins database for the investigation of sequences and structures. *J. Mol. Biol.*, **247**, 536–540.
- Noguchi,T. and Akiyama,Y. (2003) PDB-REPRDB: a database of representative protein chains from the Protein Data Bank (PDB) in 2003. *Nucleic Acids Res.*, **31**, 492–493.
- Oliveira,K.M. *et al.* (2001) Crystal structures of bovine beta-lactoglobulin in the orthorhombic space group C222(1). Structural differences between genetic

- variants A and B and features of the Tanford transition. *Eur. J. Biochem.*, **268**, 477–483.
- Paesen, G.C. *et al.* (1999) Tick histamine-binding proteins: isolation, cloning, and three-dimensional structure. *Mol. Cell*, **3**, 661–671.
- Rueda, M. *et al.* (2007) A consensus view of protein dynamics. *Proc. Natl Acad. Sci. USA*, **104**, 796–801.
- Schlessinger, A. and Rost, B. (2005) Protein flexibility and rigidity predicted from sequence. *Proteins*, **61**, 115–126.
- Song, G. and Jernigan, R.L. (2007) vGNM: a better model for understanding the dynamics of proteins in crystals. *J. Mol. Biol.*, **369**, 880–893.
- Srivastava, A. and Granek, R. (2013) Cooperativity in thermal and force-induced protein unfolding: integration of crack propagation and network elasticity models. *Phys. Rev. Lett.*, **110**, 138101.
- Szarecka, A. *et al.* (2007) Dynamics of firefly luciferase inhibition by general anesthetics: Gaussian and anisotropic network analyses. *Biophys. J.*, **93**, 1895–1905.
- Tegge, A.N. *et al.* (2009) NNcon: improved protein contact map prediction using 2D-recursive neural networks. *Nucleic Acids Res.*, **37**, W515–W518.
- Tuzmen, C. and Erman, B. (2011) Identification of ligand binding sites of proteins using the Gaussian network model. *PLoS One*, **6**, e16474.
- Vannini, A. *et al.* (2004) Crystal structure of the quorum-sensing protein TraM and its interaction with the transcriptional regulator TraR. *J. Biol. Chem.*, **279**, 24291–24296.
- Wang, Z. and Xu, J. (2013) Predicting protein contact map using evolutionary and physical constraints by integer programming. *Bioinformatics*, **29**, i266–i273.
- Wieninger, S.A. *et al.* (2011) ATP binding enables broad antibiotic selectivity of aminoglycoside phosphotransferase(3′)-IIIa: an elastic network analysis. *J. Mol. Biol.*, **409**, 450–465.
- Yang, L. *et al.* (2007a) How well can we understand large-scale protein motions using normal modes of elastic network models? *Biophys. J.*, **93**, 920–929.
- Yang, L. *et al.* (2008) Close correspondence between the motions from principal component analysis of multiple HIV-1 protease structures and elastic network modes. *Structure*, **16**, 321–330.
- Yang, L. *et al.* (2009) Protein elastic network models and the ranges of cooperativity. *Proc. Natl Acad. Sci. USA*, **106**, 12347–12352.
- Yang, L.W. and Bahar, I. (2005) Coupling between catalytic site and collective dynamics: a requirement for mechanochemical activity of enzymes. *Structure*, **13**, 893–904.
- Yang, L.W. *et al.* (2007b) Insights into equilibrium dynamics of proteins from comparison of NMR and X-ray data with computational predictions. *Structure*, **15**, 741–749.
- Yuan, Z. *et al.* (2005) Prediction of protein B-factor profiles. *Proteins*, **58**, 905–912.
- Zhang, H. *et al.* (2009) On the relation between residue flexibility and local solvent accessibility in proteins. *Proteins*, **76**, 617–636.
- Zheng, W. (2008) A unification of the elastic network model and the Gaussian network model for optimal description of protein conformational motions and fluctuations. *Biophys. J.*, **94**, 3853–3857.
- Zheng, W. (2010) Anharmonic normal mode analysis of elastic network model improves the modeling of atomic fluctuations in protein crystal structures. *Biophys. J.*, **98**, 3025–3034.
- Zheng, W. and Brooks, B.R. (2005) Normal-modes-based prediction of protein conformational changes guided by distance constraints. *Biophys. J.*, **88**, 3109–3117.
- Zheng, W. and Doniach, S. (2003) A comparative study of motor-protein motions by using a simple elastic-network model. *Proc. Natl Acad. Sci. USA*, **100**, 13253–13258.
- Zhu, F. and Hummer, G. (2010) Pore opening and closing of a pentameric ligand-gated ion channel. *Proc. Natl Acad. Sci. USA*, **107**, 19814–19819.
- Zhuravleva, A. *et al.* (2007) Propagation of dynamic changes in barnase upon binding of barstar: an NMR and computational study. *J. Mol. Biol.*, **367**, 1079–1092.